RESEARCH ARTICLE
SPACE PHYSICS: MAGNETOSPHERIC PHYSICS

Earth and Planetary Physics
6: 536–545, 2022
doi: 10.26464/epp2023002

Distribution of O^+ and O_2^+ fluxes and their escape rates in the near-Mars magnetotail: A survey of MAVEN observations

HengLe Du[1], Xing Cao[1*], BinBin Ni[1,2*], Song Fu[1], Xin Ma[1], XiaoTong Yun[1], MinYi Long[1], and Qiong Luo[1]

[1]Department of Space Physics, School of Electronic Information, Wuhan University, Wuhan 430072, China;

[2]Chinese Academy of Sciences, Center for Excellence in Comparative Planetology, Hefei 230026, China

Key Points:

- Planetary heavy ions (oxygen ions and molecular oxygen ions) in the Martian magnetotail are dominant in the tailward direction.
- Tailward heavy ion fluxes are larger in the −E (electric field) hemisphere than in the +E hemisphere.
- The escape rates of heavy ions are closely related with CIR and solar wind dynamic pressure.

Citation: Du, H. L., Cao, X., Ni, B. B., Fu, S., Ma, X., Yun, X. T., Long, M. Y., and Luo, Q. (2022). Distribution of O^+ and O_2^+ fluxes and their escape rates in the near-Mars magnetotail: A survey of MAVEN observations. *Earth Planet. Phys.*, *6*(6), 536–545. http://doi.org/10.26464/epp2023002

Abstract: Tailward ion outflows in the Martian-induced magnetotail are known to be one of the major channels for Martian atmospheric escape. On the basis of nearly 6.5 years of observations from the Mars Atmosphere and Volatile EvolutioN (MAVEN) mission, we investigate the statistical distribution of tailward and Marsward fluxes of heavy ions (i.e., O^+ and O_2^+) in the near-Mars magnetotail and explore their characteristic responses to the corotating interaction region (CIR), solar wind dynamic pressure, and local magnetic field intensity. Our results show that the tailward fluxes of oxygen ions and molecular oxygen ions in the magnetotail are significantly greater than their Marsward fluxes and that the tailward flux of molecular oxygen ions is generally larger than that of oxygen ions. Furthermore, the tailward ion flux distribution exhibits dependence on the CIR, solar wind dynamic pressure, and local magnetic field strength in a manner stronger than the Marsward ion flux distribution. According to the distribution of tailward ion fluxes, we calculate the corresponding escape rates of heavy ions and show that when the CIR occurs, the total escape rates of oxygen ions and molecular oxygen ions increase by a factor of ~2 and ~1.2, respectively. We also find that the escape rates of heavy ions increase with the enhancement of solar wind dynamic pressure, whereas the overall effect of the local magnetic field is relatively weak. Our study has important implications for improved understanding of the underlying mechanisms responsible for the Martian atmospheric escape and the evolution of the Martian atmospheric climate.

Keywords: Martian-induced magnetotail; atmospheric heavy ion outflow; corotating interaction region; escape rate

1. Introduction

Many studies have presented evidence that Mars was covered with significant amounts of liquid water in the past, implying a warm climate and an atmosphere filled with greenhouse gases (most probably CO_2) at that time (Jakosky and Phillips, 2001; Chassefière and Leblanc, 2004; Bibring et al., 2006; Barabash et al., 2007). However, the early Martian atmosphere has been lost to interplanetary space over billions of years, resulting in the transition of the Martian climate to today's harsh and uninhabitable state. Escape processes in the Martian upper atmosphere, both thermal and nonthermal, have been considered to explain the massive lack of water on Mars today (Barabash et al., 2007; Brain et al., 2016). The interaction between the solar wind and the Martian upper atmosphere is mainly considered the escape mechanism of ions, whereas Jeans escape is mainly considered the escape mechanism of light hydrogen species (Luhmann et al., 1992; Carlsson et al., 2006; Cui J et al., 2022; Gu H et al., 2022). Heavy planetary ions, produced by photoionization, electron impact, and charge exchange in the Martian ionosphere, can be accelerated by the solar wind convection electric field and partially escape from the Martian atmosphere (Lillis et al., 2015). According to a study by Chassefière and Leblanc (2004), three main nonthermal escape processes led to the loss to space of the Martian atmosphere: photochemical escape, ionospheric outflow, and ion sputtering. In addition, Dong Y et al. (2015) reported three different forms of Martian atmospheric ion escape: antisunward ion fluxes in the magnetotail region, ion plumes along the solar wind convection electric field, and upstream pickup ion fluxes.

Because of the absence of a significant global intrinsic magnetic field, the solar wind can interact directly with the upper atmosphere of Mars, where energy and particle exchanges occur between the solar wind and ionospheric plasma that can subsequently lead to ion escape. Guinan and Ribas (2004) suggested

Correspondence to: X. Cao, cxing@whu.edu.cn
B. B. Ni, bbni@whu.edu.cn
Received 24 JUN 2022; Accepted 29 AUG 2022.
Accepted article online 16 SEP 2022.

that solar radiation affects ion escape by increasing the temperature and photoionization of the Martian exosphere. By comparing the escape rates at different distances from the Sun under different solar activities, Lin RT et al. (2021) concluded that the heliocentric radial distance has a more significant effect on the escape of Martian atmospheric ions than does the activity of the solar wind. Lundin et al. (2008) suggested that increased solar radiation and solar wind dynamic pressure causes increased plasma erosion and ion escape by enhancing the energy and momentum transfer between the solar wind plasma and Martian planetary ions. Jakosky et al. (2015a) investigated the effects of interplanetary coronal mass ejection events on the escape of ions from the Martian atmosphere and found that the ion escape rate increases significantly during interplanetary coronal mass ejection events. Accordingly, the escape of ions from the Martian atmosphere is strongly dependent on the parameters of the solar wind. Solar rotation enables a fast stream to catch up with a preceding slow stream, creating a corotating interaction region (CIR). Corotating interaction region events represent a significant increase in the solar wind proton density, velocity, and temperature as well as the solar wind dynamic pressure and energy flux (Nilsson et al., 2012; Wang ZH et al., 2018; Huang H et al., 2019). Previous measurements of ion escape rates in response to CIRs have been reported by Edberg et al. (2010) using Mars Express data, which estimated a 2.5 order of magnitude increase in planetary ion escape during CIR events. Nilsson et al. (2011) also studied the influence of CIR events on ion escape and found that the fluxes of escaping planetary heavy ions increase significantly when a CIR occurs.

Mars is a planet with a local crustal magnetic field, the presence of which is thought to be another important factor that affects ion escape (Connerney et al., 2001; Brain et al., 2010; Lundin et al., 2011; Fang XH et al., 2015; Ramstad et al., 2016). Nilsson et al. (2011) proposed that the escape from the southern hemisphere is approximately 33% less than that from the northern hemisphere because of the presence of significant crustal magnetic fields in the south. Using nearly 8 years of ion flux statistics from Mars Express, Ramstad et al. (2016) showed that the dayside orientation of the crustal field has a significant effect on the escape rate of atmospheric ions. Fang XH et al. (2010) simulated and quantified the effect of the crustal magnetic field on ion escape by using a newly developed ion transport model. Their results showed that both the spatial distribution and the escape rate of ions are affected by the local magnetic field. Dubinin et al. (2017) revealed that the Martian magnetosphere has different types of open and closed magnetic field lines and that the closed magnetic field lines in the near-Mars magnetotail may be an explanation for inhibiting the ion escape. In contrast, Inui et al. (2018) speculated that heavy ions of the Martian ionosphere may be gradually transported upward along the open magnetic field lines and flow toward the magnetotail, causing the planetary ions to escape. However, the effect of local magnetic fields on the escape of Martian atmospheric ions still remains to be fully understood.

In this study, we statistically study the relationships between heavy ion escape and CIR events, solar wind dynamic pressure, and the local magnetic field in the Martian magnetotail by calculating the tailward and Marsward ion fluxes and escape rates. The structure of this paper is organized as follows: we introduce the instruments on board the Mars Atmosphere and Volatile Evolution (MAVEN) spacecraft and the data set used in this study in Section 2. We present a representative example of heavy ion outflow in the Martian magnetotail observed by MAVEN on February 11, 2016, in Section 3. In Section 4, the statistical distributions of Martian tailward fluxes of suprathermal (>25 eV) heavy ions and the corresponding heavy ion escape rates are reported to investigate the dependence of heavy ion escape on CIR events, the solar wind dynamic pressure, and the local magnetic field. Finally, the results are summarized by comparing different ion escape mechanisms.

2. Instrumentation and Data Analysis

The MAVEN spacecraft carries nine sensors (Jakosky et al., 2015b), which allowed us to obtain the spatial distribution of planetary ions and investigate the potential mechanisms that are responsible for the ion escape processes from Mars, with the aim of understanding the escape processes from Mars. The Suprathermal and Thermal Ion Composition (STATIC) instrument (McFadden et al., 2015) is designed to measure energy-angular distributions of positive ions and the ion mass compositions that can distinguish different ion species from Mars, including H^+, O^+, O_2^+, and CO_2^+. The STATIC instrument can produce 22 different products with different mass, energy, angular, and time resolutions. In this paper, we mainly used "d0" data products (32 energy steps, 4 deflection angles, 16 azimuthal anodes, and 8 mass bins). We used magnetometer data (Connerney et al., 2015) to obtain the background magnetic field intensity in Mars-centered Solar Orbital (MSO) coordinates, and we used data with a time resolution of 1 s. The solar wind ion analyzer (Halekas et al., 2015) is an instrument used to measure the properties of solar wind ions, including their velocity and density. Here, we derived the upstream solar wind dynamic pressure data from solar wind ion analyzer measurements.

In this study, MAVEN data in Mars-Solar-Orbital (MSO) and Mars-Solar-Electric field (MSE) coordinates are used. The MSO coordinate is defined with the x-axis pointing toward the Sun, the z-axis perpendicular to the ecliptic plane pointing to the northern hemisphere, and the y-axis completing the right-handed system. To investigate the effects of the solar wind convection electric field on magnetotail heavy ion escape, the statistical results of planetary heavy ions are obtained in the MSE coordinate system: the x-axis points from Mars to the Sun, the z-axis is oriented toward the solar wind convection electric field ($E_{sw} = -V_{sw} \times B_{sw}$), and the y-axis completes the right-handed system. We deduced that the MSE coordinate system could be obtained by rotating the MSO coordinate system around the x-axis by a certain angle, which is determined by the interplanetary magnetic field orientation. We took the interplanetary magnetic field orientation on each MAVEN orbit by averaging the magnetometer data in the upstream solar wind within two consecutive orbits. However, MAVEN has not always been able to measure data from the upstream solar wind because of changes in the probe's orbit. To ensure the validity of the data, if the time duration that MAVEN flew in the region of the solar wind was less than 20 minutes, the measurements from this orbit were not used. At the same time, we removed the 10-minute jitter error on both sides of the solar wind boundary from the magnetometer and the upstream solar wind data.

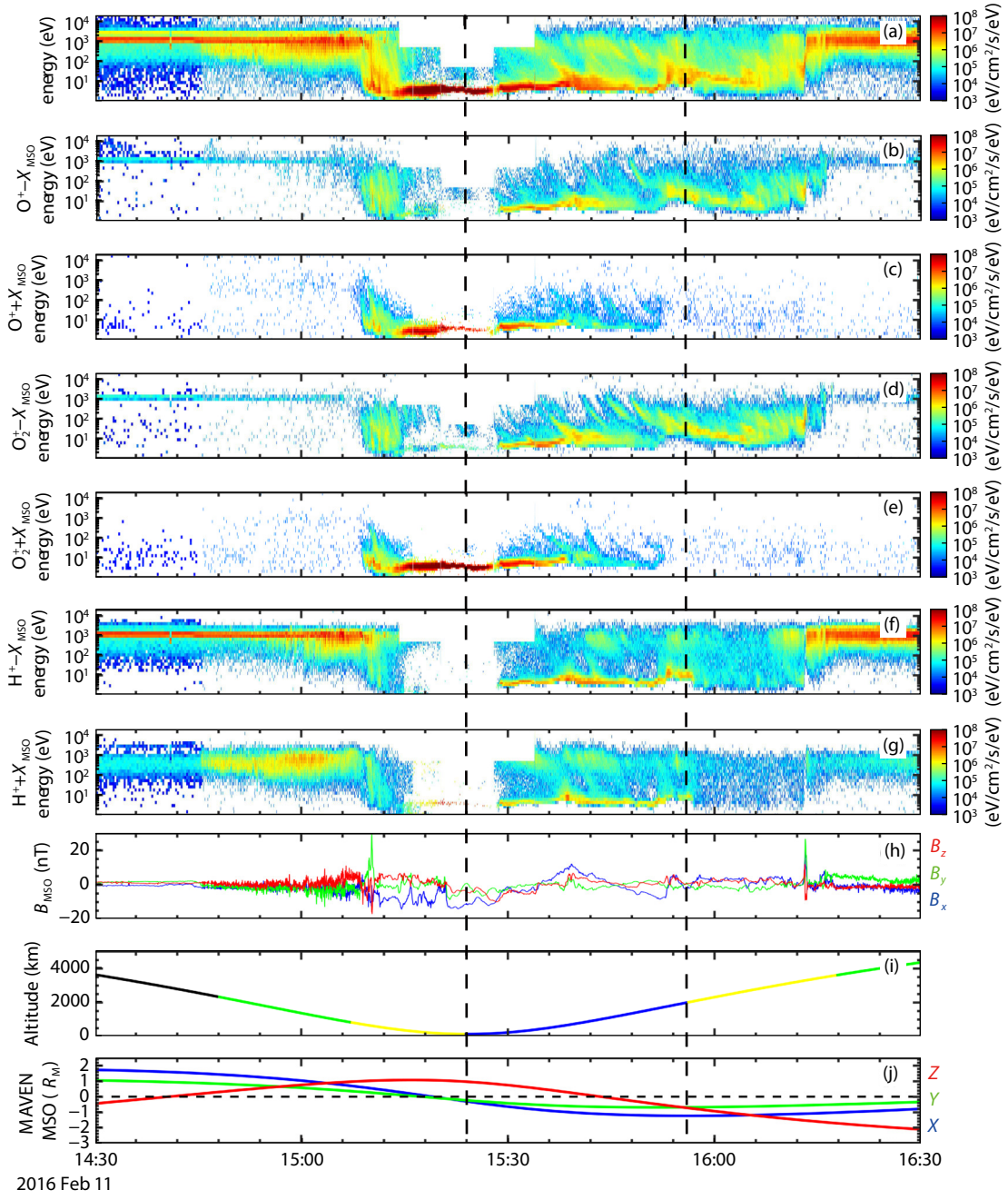

Figure 1. Time series plot of charged particles and magnetic fields observed by MAVEN on February 11, 2016. From top to bottom, the seven upper panels display STATIC energy spectra for (a) all ions, (b) tailward oxygen ions, (c) Marsward oxygen ions, (d) tailward molecular oxygen ions, (e) Marsward molecular oxygen ions, (f) tailward protons, and (g) Marsward protons. The three lower panels depict the (h) magnetic field in Mars-centered Solar Orbital (MSO) coordinates from the magnetometer, (i) spacecraft altitude in which colors show the nominal plasma regions, and (j) spacecraft position in the MSO frame. The vertical dashed lines denote the boundaries of the Martian wake ($\rho_{MSO} \equiv \sqrt{Y_{MSO}^2 + Z_{MSO}^2} < 1R_M$ and $X_{MSO} < 0$).

3. MAVEN Observations

We begin our analysis with a typical example (Figure 1) of primarily tailward-moving heavy ions in the Martian magnetotail region observed by MAVEN on February 11, 2016. From top to bottom, the seven upper panels in Figure 1 show energy–time spectrograms for (a) all ions, (b) tailward oxygen ions, (c) Marsward oxygen ions, (d) tailward molecular oxygen ions, (e) Marsward molecular oxygen ions, (f) tailward protons, and (g) Marsward protons. The three lower panels depict the (h) magnetic field in MSO coordinates from the magnetometer, (i) spacecraft altitude, and (j) spacecraft position in the MSO frame. In this case, MAVEN passed from the solar wind through the magnetosheath, from the induced magnetosphere into the magnetotail wake region, and finally exited the magnetosheath region during the outbound pass. The colors in Figure 1i show the nominal plasma regions, where the green, yellow, and blue lines represent the magne-

tosheath, the induced magnetosphere, and the magnetotail wake region, respectively. The determination of the nominal plasma regions are from Trotignon's model (Trotignon et al., 2006). A notable feature of the transition from the magnetosheath to the induced magnetosphere shown in the figure is the conversion of solar wind protons to planetary heavy ions, which is consistent with previous studies (e.g., Xu SS et al., 2016a; Halekas et al., 2017; Matsunaga et al., 2017; Cui J et al., 2020).

Specifically, we concentrate on the angle-integrated, directional energy spectra of the ions mentioned above in the Martian magnetotail region. Figures 1f and 1g show that the energy spectra of hydrogen ions cover a wide range of energy in the Martian magnetotail. For the thermal hydrogen ions with energies up to 2 keV in the magnetotail, their energies are close to those of solar wind protons, implying that these thermal ions are derived from the magnetosheath region and ultimately from the solar wind. In contrast, cold protons with energies below 10 eV appear in the altitude range of 100–1,000 km, suggesting that they are produced in the ionosphere. The energy spectra of oxygen ions and molecular oxygen ions show similar phenomena in the tailward and Marsward directions. In general, planetary heavy ions (oxygen ions and molecular oxygen ions) are mainly distributed in near-Mars space with energies of ~10–100 eV. It has been suggested that both cold and high-energy tailward heavy ions originate from the ionosphere but that the latter are generated by accelerating ions to gain escape energy (Inui et al., 2019). It is worth noting that the tailward flux of planetary heavy ions (Figures 1b and 1d) in the Martian wake is significantly larger than the Marsward flux (Figures 1c and 1e), indicating the escape of planetary heavy ions. A possible explanation for the tailward heavy ions is the transport of heavy ions to the magnetotail along the magnetic field lines owing to day–night magnetic connectivity (Xu SS et al., 2016b; Cao YT et al., 2020).

4. Statistical Results

According to MAVEN observations, the main escaping heavy ion species in the near-Mars magnetotail are oxygen ions and molecular oxygen ions, whereas CO_2^+ represents a minor fraction of the heavy ion outflow from Mars (Lundin et al., 2009; Inui et al., 2018). Therefore, we focused on the flux distribution of oxygen ions and molecular oxygen ions in the Martian magnetotail in this study to investigate the characteristics of heavy ion escape. Figure 2 shows *YZ*-MSE maps of directional heavy ion fluxes with energy greater than 25 eV in the near-Mars magnetotail ($\rho_{MSO} < 1.5R_M$ and $-1.5R_M < X_{MSO} < -1R_M$) for the time period from December 2014 to May 2021. It is worth noting that the data can provide sufficient spatial coverage without an obvious uneven or asymmetric distribution. Large differences between Marsward heavy ion fluxes (Figures 2a and 2c) and tailward heavy ion fluxes (Figures 2b and 2d) suggest that the net heavy ion fluxes are dominated by escaping heavy ions, which is generally consistent with the work of Inui et al. (2019). This remarkable comparison provides strong evidence that the Martian magnetotail acts as a channel for heavy ion escape. In addition, we observe that tailward heavy ion fluxes are larger in the –E (electric field) hemisphere than in the +E hemisphere. Dubinin et al. (2018) believed that the ionosphere expands in the –E hemisphere compared with the +E hemisphere, resulting in more heavy ion outflows observed in the –E hemisphere. The

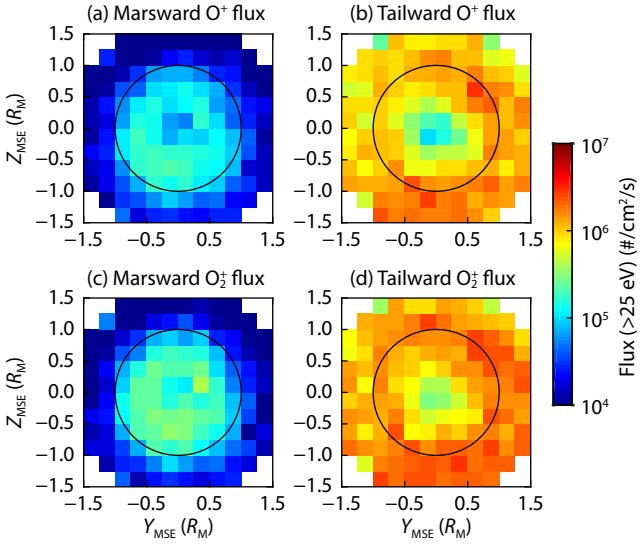

Figure 2. *YZ*-MSE maps of the average integral fluxes ($cm^{-2}{\cdot}s^{-1}$) of heavy planetary ions with E >25 eV in the near-Mars magnetotail ($\rho_{MSO} < 1.5R_M$ and $-1.5R_M < X_{MSO} < -1R_M$) for the time period from December 2014 to May 2021. (a) Marsward and (b) tailward oxygen ions; (c) Marsward and (d) tailward molecular oxygen ions. Each 0.25 $R_M \times 0.25$ R_M bin displays average fluxes. MSE, Mars–Solar–Electric field coordinate system; MSO, Mars-centered Solar Orbital coordinate system.

characteristics of the distributions in Figures 2b and 2d are very similar, implying that their escape mechanisms are basically the same. It is clear that molecular oxygen ion fluxes are generally larger than the oxygen ion fluxes. Magnetohydrodynamic simulations conducted by Liu Y et al. (2001) showed that the most abundant ion species in the escaping plasma from the Martian tail were molecular oxygen ions. Figure 2 also shows that Marsward heavy ion fluxes are mainly distributed inside the wake, whereas tailward heavy ion fluxes are mainly outside the wake region. Thus, we suggest that the planetary heavy ions escaping from the magnetotail originate from the ions produced by photoionization and charge exchange on the dayside of Mars.

As mentioned, the CIR has great effects on the atmosphere of Mars in terms of the loss of heavy ions. Figure 3 shows the fluxes of directional heavy ions with energy greater than 25 eV in the near-Mars magnetotail ($\rho_{MSO} < 1.5R_M$ and $-1.5R_M < X_{MSO} < -1R_M$) projected into the MSE coordinates in the *y*–*z* plane during the passing of CIRs and during normal solar wind conditions. The data from CIR events are based on all CIRs identified by Huang H et al. (2019) between December 2014 and November 2018. We set a threshold of 50 for the sample number in each bin. For bins with a data density less than 50, the data were not used. Although the data coverage is slightly insufficient for a precise comparison, a significant increase in tailward heavy ion fluxes can still be observed as the CIR passes by, which is consistent with the observations of Edberg et al. (2010). The larger tailward heavy ion fluxes in the magnetotail corresponding to the CIR events suggest that CIRs can drive the erosion of the upper atmosphere by significantly increasing the escape of heavy planetary ions from Mars.

Figure 4 shows how directional heavy ion fluxes in the tail ($\rho_{MSO} <$

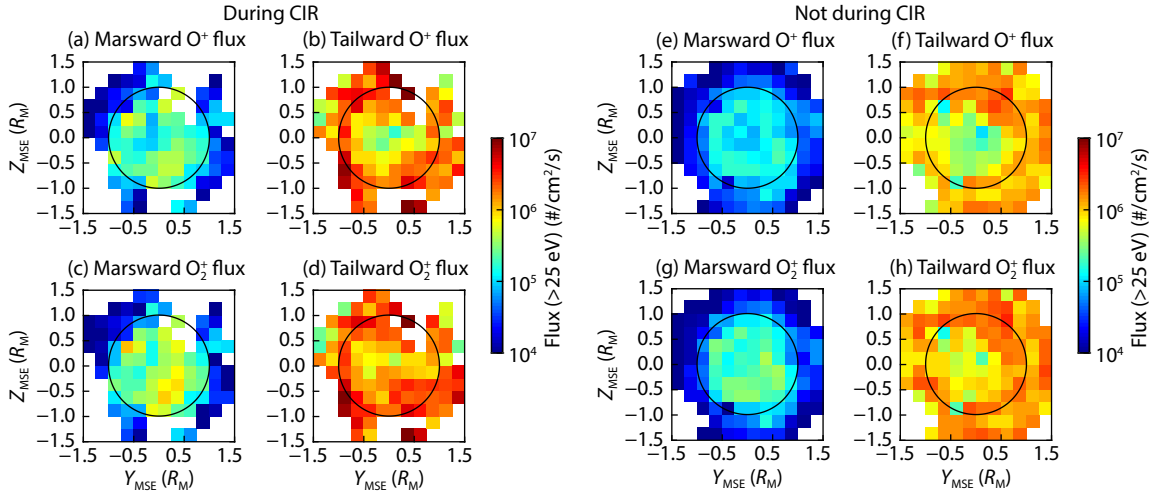

Figure 3. *YZ*-MSE maps of the average integral fluxes ($cm^{-2}·s^{-1}$) of heavy planetary ions with E >25 eV in the near-Mars magnetotail ($\rho_{MSO} < 1.5R_M$ and $-1.5R_M < X_{MSO} < -1R_M$) during (a–d) the passing of corotating interaction regions (CIRs), and during (e–h) "normal" solar wind conditions for the time period from December 2014 to November 2018. The left four panels show (a) Marsward and (b) tailward oxygen ions during CIR events; and (c) Marsward and (d) tailward molecular oxygen ions during CIR events. The right four panels show (e) Marsward and (f) tailward oxygen ions during "normal" solar wind conditions; and (g) Marsward and (h) tailward molecular oxygen ions during "normal" solar wind conditions. MSE, Mars–Solar–Electric field coordinate system; MSO, Mars-centered Solar Orbital coordinate system.

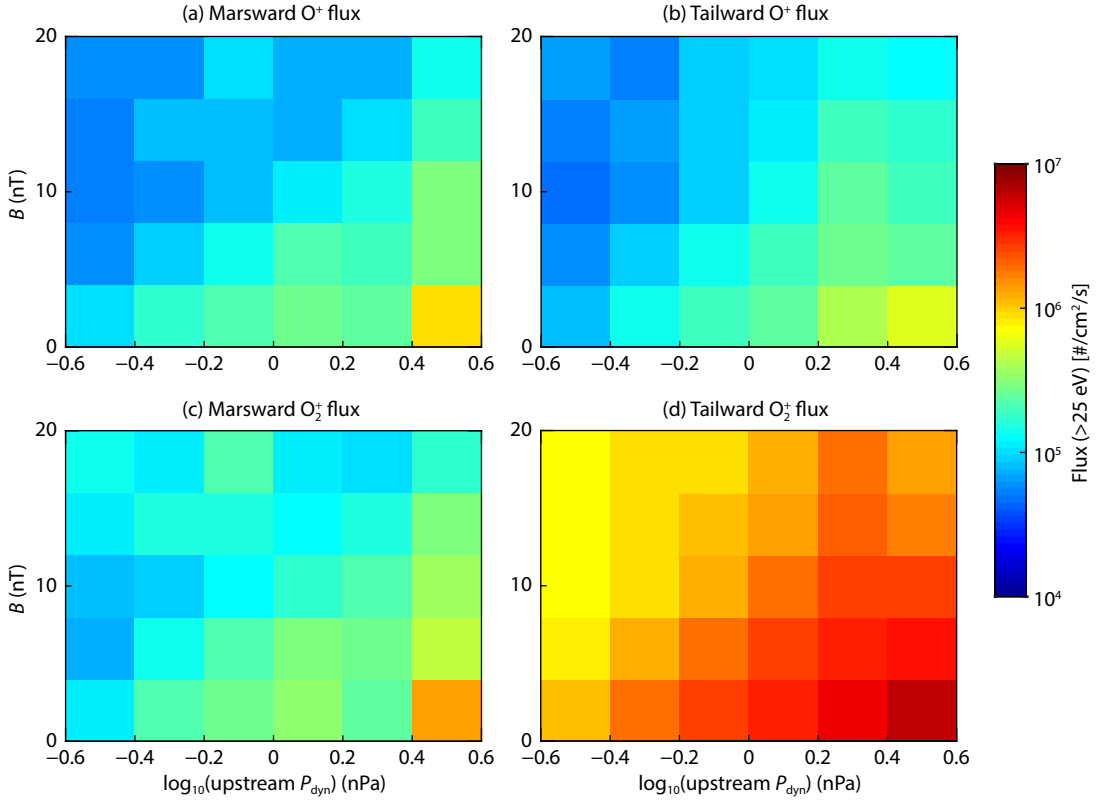

Figure 4. Maps of the average integral fluxes ($cm^{-2}·s^{-1}$) of heavy planetary ions with E >25 eV in the tail ($\rho_{MSO} < 1.5R_M$ and $-1.5R_M < X_{MSO} < -1R_M$) as a function of local magnetic field intensity and upstream dynamic pressure. Each panel shows (a) Marsward and (b) tailward oxygen ions; and (c) Marsward and (d) tailward molecular oxygen ions. The data used here are the same as those in Figure 2. MSE, Mars–Solar–Electric field coordinate system; MSO, Mars-centered Solar Orbital coordinate system.

$1.5R_M$ and $-1.5R_M < X_{MSO} < -1R_M$) vary with the variations in the solar wind dynamic pressure and the local magnetic field intensity. The heavy ion fluxes can be seen to increase with increasing solar wind dynamic pressure, especially for tailward oxygen ions and molecular oxygen ions (Figures 4b and 4d), implying that the condition of high solar wind dynamic pressure accelerates the planetary ion escape. Furthermore, we observed that larger heavy ion fluxes appear in the relatively weak magnetic field region, a

feature in agreement with the statistical results of Harada et al. (2015), who proposed that a plasma sheet with a small magnetic field is the source of escaped ions. Xu SS et al. (2016a) concluded that Martian magnetotail ion escape is concentrated not only in the current sheet but also in the magnetic lobe region. Our statistical results indicate that a magnetic lobe with a small magnetic field can also be the source of escaped ions.

To better understand the relationship between the fluxes of heavy ions and the upstream solar wind dynamic pressure, we classified the flux data into three parts according to the solar wind dynamic pressure shown in Figure 4: a low pressure condition ($-0.6 < \log_{10}(P_{dyn}) < -0.2$, Figures 5a and 5d), a moderate pressure condition ($-0.2 < \log_{10}(P_{dyn}) < 0.2$, Figures 5b and 5e), and a high pressure condition ($0.2 < \log_{10}(P_{dyn}) < 0.6$, Figures 5c and 5f). By comparing the escape heavy ion fluxes in the tail from low (Figures 5a and 5d) to high solar wind dynamic pressure (Figures 5c and 5f) , we could observe a general increase in the ion fluxes in the tail region as the dynamic pressure increases. Therefore, the conclusion can be drawn that the contribution of the solar wind dynamic pressure is positively correlated with the outflow of planetary heavy ions.

Here, we utilize the same method described above to study the dependence of the heavy ion fluxes in the tail on the Martian local magnetic field. Figure 6 shows the statistical distribution of heavy ions corresponding to three different ranges of local magnetic field intensities, namely, low magnetic field strength ($0\ \text{nT} < |B| <$

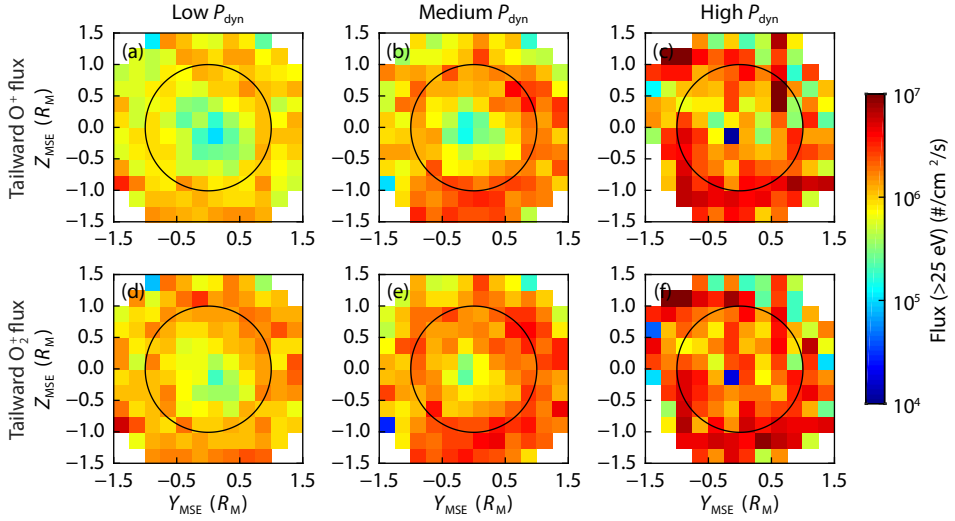

Figure 5. *YZ*-MSE maps of the average integral fluxes ($cm^{-2}\cdot s^{-1}$) of tailward (a–c) oxygen ions and (d–f) molecular oxygen ions with E >25 eV in the near-Mars wake ($\rho_{MSO} < 1.5R_M$ and $-1.5R_M < X_{MSO} < -1R_M$). The flux data are divided by the intensity of the upstream dynamic pressure: (a, d) low ($-0.6 < \log_{10}(P_{dyn}) < -0.2$); (b, e) medium ($-0.2 < \log_{10}(P_{dyn}) < 0.2$); (c, f) high ($0.2 < \log_{10}(P_{dyn}) < 0.6$) upstream dynamic pressure. MSE, Mars–Solar–Electric field coordinate system; MSO, Mars-centered Solar Orbital coordinate system.

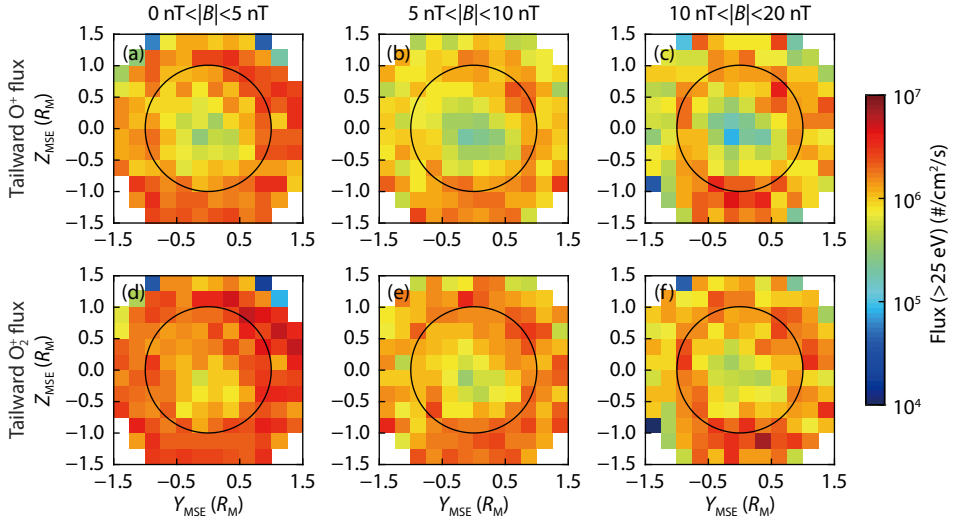

Figure 6. *YZ*-MSE maps of the average integral fluxes ($cm^{-2}\cdot s^{-1}$) of tailward (a–c) oxygen ions and (d–f) molecular oxygen ions with E >25 eV in the near-Mars wake ($\rho_{MSO} < 1.5\ R_M$ and $-1.5\ R_M < X_{MSO} < -1\ R_M$). Data are divided by the local magnetic field intensity presented: (a, d) weak ($0\ \text{nT} < |B| < 5\ \text{nT}$); (b, e) medium ($5\ \text{nT} < |B| < 10\ \text{nT}$); (c, f) strong ($10\ \text{nT} < |B| < 20\ \text{nT}$) local magnetic field. MSE, Mars–Solar–Electric field coordinate system; MSO, Mars-centered Solar Orbital coordinate system.

5 nT, Figures 5a and 5d), moderate magnetic field strength (5 nT < $|B|$ < 10 nT, Figures 5b and 5e), and high magnetic field strength (10 nT < $|B|$ < 20 nT, Figures 5c and 5f). The main feature of the distribution of ion fluxes is that the larger heavy ion fluxes are observed during the lower local magnetic field condition, whereas relatively small heavy ion fluxes are observed during the medium and high magnetic field conditions. Weakly magnetized planets like Mars, which lacks the protection of a global magnetic field, seem to be less able to withstand the impact of blows from the intense solar wind. Note that the differences in the distribution of heavy ion fluxes in the near-Mars wake region are less pronounced between the medium local magnetic field and the strong local magnetic field.

We have shown that oxygen ion and molecular oxygen ion flux distributions in the magnetotail correlate differently with upstream solar wind and local magnetic field parameters. Until now, we have exhibited and analyzed only the ion flux statistics. Here, we calculate the total escape rates of the heavy ions under different solar wind and local magnetic field conditions and compare these escape rates to further validate their correlation. By integrating the maps of the planetary ion flux distribution in the y–z plane of the MSE coordinates (Barabash et al., 2007), as shown in Figures 3, 5, and 6 respectively, we obtain the corresponding total escape rates. It is worth noting that the flux data coverage for the CIR and non-CIR cases is slightly different. We interpolate regions of missing data with the mean of the flux data to guarantee a more accurate escape rate.

Figure 7 shows the escape rates of Martian planetary heavy ions under CIR and non-CIR events, different solar wind dynamic pressures, and different local magnetic fields, respectively. As shown in Figure 7a, the total escape rate of oxygen ions is observed to increase significantly by a factor of ~2 and molecular oxygen ions by a factor of ~1.2 during the CIR events, suggesting that the CIR can significantly enhance the escape of heavy ions from the Martian atmosphere. Besides CIR events, a strong correlation also exists between the upstream solar wind dynamic pressure and the total escape rate of heavy ions. As the solar wind dynamic pressure gradually increases, the total escape rate of oxygen ions and molecular oxygen ions also increases in a similar trend, and their escape rates reach a maximum of 2.44×10^{24} s^{-1} and 2.50×10^{24} s^{-1}, respectively, under the condition of high solar wind dynamic pressure (Figure 7b). This positive correlation between the solar wind dynamic pressure and the planetary ion escape rate indicates that higher solar wind pressure pushes more ions to escape. Furthermore, CIR events can significantly raise the solar wind dynamic pressure. We noted that the solar wind dynamic pressure and CIR events are both important for planetary ion escape. Nevertheless, the influence of local magnetic field intensity variations on the escape of heavy ions is quite different from that of the solar wind dynamic pressure. When the local magnetic field increases from low to moderate intensity, the escape rates of oxygen ions and molecular oxygen ions decrease from the highest at 1.44×10^{24} s^{-1} and 1.98×10^{24} s^{-1} to 0.98×10^{24} s^{-1} and 1.34×10^{24} s^{-1}, respectively, and remain almost unchanged as the local magnetic field increases to a high intensity. This trend implies that a weak local magnetic field favors the escape of planetary ions, whereas a stronger magnetic field seems to act as a protective barrier to the Martian space environment, preventing their escape.

5. Conclusions and Discussion

In this study, using nearly 6.5 years of MAVEN observations, we have presented the statistical distribution of tailward and Marsward heavy ion (i.e., O^+ and O_2^+) fluxes in the Martian magnetotail under different conditions of CIRs, solar wind dynamic pressures, and local magnetic fields and have calculated the corresponding escape rates of Martian planetary heavy ions. The major conclusions are summarized as follows:

(1) Tailward oxygen ion and molecular oxygen ion fluxes are much higher than their Marsward fluxes, indicating that heavy ions

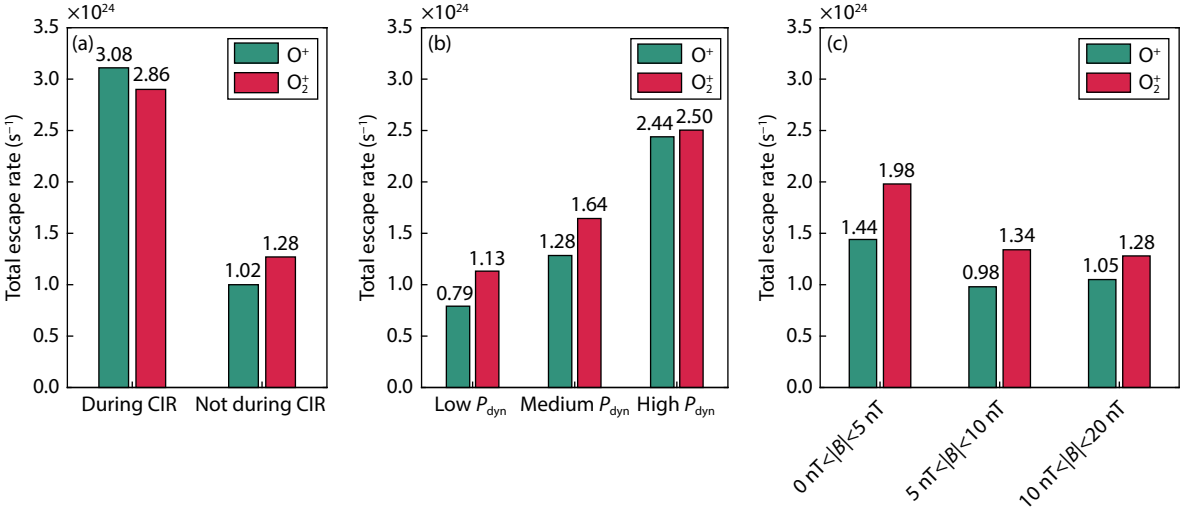

Figure 7. Total escape rates of planetary heavy ions with E >25 eV in the near Martian tail ($\rho_{MSO} < 1.5R_M$ and $-1.5R_M < X_{MSO} < -1R_M$) are divided into (a) corotating interaction region (CIR) and non-CIR, (b) different solar wind dynamic pressure conditions, and (c) different local magnetic field intensities.

escape from the Martian magnetotail. In general, both the tailward and Marsward fluxes of molecular oxygen ions are larger than those of oxygen ions.

(2) The tailward heavy ion fluxes in the −E (electric field) hemisphere are significantly larger than those in the +E hemisphere, which is related to the solar wind convection electric field. The tailward heavy ion fluxes increase significantly during the CIR periods, and large tailward heavy ion fluxes are more likely to occur with a weak magnetic field and high solar wind dynamic pressure.

(3) For CIR events, the escape rates can reach maximum values of 3.08×10^{24} s^{-1} for oxygen ions and 2.86×10^{24} s^{-1} for molecular oxygen ions, corresponding to an increase by a factor of ~2 and ~1.2, respectively. The escape rates of planetary heavy ions increase with an increase in the solar wind dynamic pressure, whereas the overall effect of the local magnetic field is relatively weak.

From these results, we suggest the escape process of Martian atmospheric space is a complex coaction of many factors and cannot be attributed to a single factor. Our study has demonstrated that both CIR events and high solar wind dynamic pressure make important contributions to Martian planetary ion escape. When the total escape rates during CIR events are compared with those under high solar wind dynamic pressure, we find that heavy ion escape rates are higher when CIR occurs, indicating that the effects of CIR events are larger than those of the solar wind dynamic pressure. Although the exact mechanism of how CIR affects ion escape remains uncertain, some possible explanations have been proposed. The shocks of CIRs accelerate the ionization of the Martian ionosphere, which lacks the protection of an intrinsic global magnetic field, leading to the excitation of ionospheric plasmas that may be the main sources of escaped ions (Mendillo et al., 2006; Morgan et al., 2010). Dubinin et al. (2009) proposed that a CIR impact gives rise to ionospheric fragmentation and that ions in these regions gain energy that far exceeds the escape energy, leading to a more than 10-fold enhancement of planetary ion escape from the Martian atmosphere.

The global dipole field normally acts as a shield against the solar wind, preventing high-energy particles from penetrating and eroding the atmosphere. Because Mars does not have a global dipole magnetic field, the local magnetic field plays an important role in ion escape processes (Li SB et al., 2020). However, a detailed explanation of the complex dependence of the Martian magnetotail escape rate on the local magnetic field is beyond the scope of this study. Weber et al. (2021) suggested that the presence of a local-scale magnetic shielding suppresses local ion escape in some cases by up to 80%. An analysis of the statistical results by Lundin et al. (2011) suggests that dayside "mini-magnetospheres" can play an important role in reducing tail transport and escape of the ionospheric plasma. Thus, we can extrapolate that the small escape rate for the high magnetic field intensity is due to the enhanced shielding of the ionosphere by the local fields. Furthermore, the local crustal fields that normally withstand solar wind erosion may be completely overwhelmed during periods of increased solar wind pressure (Weber et al., 2021), which could explain the greater effect on ion escape of the solar wind dynamic pressure than the local magnetic fields.

Acknowledgments

This work was supported by the National Natural Science Foundation of China (grants 42025404, 42188101, 41904144, and 41674163), the preresearch projects on Civil Aerospace Technologies (grants D020303, D020104, and D020308) funded by the China National Space Administration, the B-type Strategic Priority Program of the Chinese Academy of Sciences (grant XDB41000000), and the Fundamental Research Funds for the Central Universities (grants 2042021kf1045 and 2042021kf1056). We thank all MAVEN mission team members for providing the data available through the NASA Planetary Data System (https://pds.nasa.gov).

References

Barabash, S., Fedorov, A., Lundin, R., and Sauvaud, J. A. (2007). Martian atmospheric erosion rates. *Science*, *315*(5811), 501–503. https://doi.org/10.1126/science.1134358

Bibring, J. P., Langevin, Y., Mustard, J. F., Poulet, F., Arvidson, R., Gendrin, A., Gondet, B., Mangold, N., Pinet, P., … Neukum, G. (2006). Global mineralogical and aqueous Mars history derived from OMEGA/Mars express data. *Science*, *312*(5772), 400–404. https://doi.org/10.1126/science.1122659

Brain, D. A., Baker, A. H., Briggs, J., Eastwood, J. P., Halekas, J. S., and Phan, T. D. (2010). Episodic detachment of Martian crustal magnetic fields leading to bulk atmospheric plasma escape. *Geophys. Res. Lett.*, *37*(14), L14108. https://doi.org/10.1029/2010GL043916

Brain, D. A., Bagenal, F., Ma, Y. J., Nilsson, H., and Stenberg Wieser, G. (2016). Atmospheric escape from unmagnetized bodies. *J. Geophys. Res.: Planets*, *121*(12), 2364–2385. https://doi.org/10.1002/2016JE005162

Cao, Y. T., Cui, J., Wu, X. S., and Zhong, J. H. (2020). Photoelectron pitch angle distribution near Mars and implications on cross terminator magnetic field connectivity. *Earth Planet. Phys.*, *4*(1), 17–22. https://doi.org/10.26464/epp2020008

Carlsson, E., Fedorov, A., Barabash, S., Budnik, E., Grigoriev, A., Gunell, H., Sauvaud, J. A., Lundin, R., Futaana, Y., … Dierker, C. (2006). Mass composition of the escaping plasma at Mars. *Icarus*, *182*(2), 320–328. https://doi.org/10.1016/j.icarus.2005.09.020

Chassefière, E., and Leblanc, F. (2004). Mars atmospheric escape and evolution; interaction with the solar wind. *Planet. Space Sci.*, *52*(11), 1039–1058. https://doi.org/10.1016/j.pss.2004.07.002

Connerney, J. E. P., Acuña, M. H., Wasilewski, P. J., Kletetschka, G., Ness, N. F., Rème, H., Lin, R. P., and Mitchell, D. L. (2001). The global magnetic field of Mars and implications for crustal evolution. *Geophys. Res. Lett.*, *28*(21), 4015–4018. https://doi.org/10.1029/2001GL013619

Connerney, J. E. P., Espley, J., Lawton, P., Murphy, S., Odom, J., Oliversen, R., and Sheppard, D. (2015). The MAVEN magnetic field investigation. *Space Sci. Rev.*, *195*(1–4), 257–291. https://doi.org/10.1007/s11214-015-0169-4

Cui, J., Gu, H., and Huang, X. (2022). Present-day atomic hydrogen escape on Mars and its variability. *Sci. Sin.: Phys., Mech. Astrono.*, *52*(3), 239502. https://doi.org/10.1360/SSPMA-2021-0290

Cui, J., Rong, Z. J., Wei, Y., and Wang, Y. M. (2020). Recent investigations of the near-Mars space environment by the planetary aeronomy and space physics community in China. *Earth Planet. Phys.*, *4*(1), 1–3. https://doi.org/10.26464/epp2020001

Dong, Y., Fang, X., Brain, D. A., McFadden, J. P., Halekas, J. S., Connerney, J. E., Curry, S. M., Harada, Y., Luhmann, J. G., and Jakosky B. M. (2015). Strong plume fluxes at Mars observed by MAVEN: an important planetary ion escape channel. *Geophys. Res. Lett.*, *42*(21), 8942–8950. https://doi.org/10.1002/2015GL065346

Dubinin, E., Fraenz, M., Woch, J., Duru, F., Gurnett, D., Modolo, R., Barabash, S., and Lundin, R. (2009). Ionospheric storms on Mars: impact of the corotating interaction region. *Geophys. Res. Lett.*, *36*(1), L01105. https://doi.org/10.1029/2008GL036559

Dubinin, E., Fraenz, M., Pätzold, M., McFadden, J., Halekas, J. S., DiBraccio, G. A., Connerney, J. E. P., Eparvier, F., Brain, D., … Zelenyi, L. (2017). The effect of solar wind variations on the escape of oxygen ions from Mars through different channels: MAVEN observations. *J. Geophys. Res.: Space Phys.*, *122*(11), 11285–11301. https://doi.org/10.1002/2017JA024741

Dubinin, E., Fraenz, M., Pätzold, M., McFadden, J., Halekas, J. S., Connerney, J. E. P., Jakosky, B. M., Vaisberg, O., and Zelenyi, L. (2018). Martian ionosphere observed by MAVEN. 3. Influence of solar wind and IMF on upper ionosphere. *Planet. Space Sci.*, *160*, 56–65. https://doi.org/10.1016/j.pss.2018.03.016

Edberg, N. J. T., Nilsson, H., Williams, A. O., Lester, M., Milan, S. E., Cowley, S. W. H., Fränz, M., Barabash, S., and Futaana, Y. (2010). Pumping out the atmosphere of Mars through solar wind pressure pulses. *Geophys. Res. Lett.*, *37*(3), L03107. https://doi.org/10.1029/2009GL041814

Fang, X. H., Liemohn, M. W., Nagy, A. F., Luhmann, J. G., and Ma, Y. J. (2010). On the effect of the Martian crustal magnetic field on atmospheric erosion. *Icarus*, *206*(1), 130–138. https://doi.org/10.1016/j.icarus.2009.01.012

Fang, X. H., Ma, Y. J., Brain, D., Dong, Y. X., and Lillis, R. (2015). Control of Mars global atmospheric loss by the continuous rotation of the crustal magnetic field: a time-dependent MHD study. *J. Geophys. Res.: Space Phys.*, *120*(12), 10926–10944. https://doi.org/10.1002/2015JA021605

Gu, H., Cui, J., Huang, X., and Sun, M. Y. (2022). Wind-enhanced hydrogen escape on Mars. *Geophys. Res. Lett.*, *49*(10), e2022GL098312. https://doi.org/10.1029/2022GL098312

Guinan, E. F., and Ribas, I. (2004). Evolution of the solar magnetic activity over time and effects on planetary atmospheres. *IAU Symp.*, *219*, 423–430. https://ui.adsabs.harvard.edu/abs/2004IAUS..219..423G

Halekas, J. S., Taylor, E. R., Dalton, G., Johnson, G., Curtis, D. W., McFadden, J. P., Mitchell, D. L., Lin, R. P., and Jakosky, B. M. (2015). The solar wind ion analyzer for MAVEN. *Space Sci. Rev.*, *195*(1–4), 125–151. https://doi.org/10.1007/s11214-013-0029-z

Halekas, J. S., Ruhunusiri, S., Harada, Y., Collinson, G., Mitchell, D. L., Mazelle, C., McFadden, J. P., Connerney, J. E. P., Espley, J. R., … Jakosky, B. M. (2017). Structure, dynamics, and seasonal variability of the Mars–solar wind interaction: MAVEN Solar Wind Ion Analyzer in-flight performance and science results. *J. Geophys. Res.: Space Phys.*, *122*(1), 547–578. https://doi.org/10.1002/2016JA023167

Harada, Y., Halekas, J. S., McFadden, J. P., Mitchell, D. L., Mazelle, C., Connerney, J. E. P., Espley, J., Larson, D. E., Brain, D. A., … Jakosky, B. M. (2015). Marsward and tailward ions in the near-Mars magnetotail: MAVEN observations. *Geophys. Res. Lett.*, *42*(21), 8925–8932. https://doi.org/10.1002/2015GL065005

Huang, H., Guo, J. P., Wang, Z. H., Lin, H. B., Zheng, J. C., Cui, J., Xu, X. J., Wang, Y., Feng, X. S., … Wan, W. X. (2019). Properties of stream interactions and their associated shocks near 1.52 au: MAVEN observations. *Astrophys. J.*, *879*(2), 118. https://doi.org/10.3847/1538-4357/ab25e9

Inui, S., Seki, K., Namekawa, T., Sakai, S., Brain, D. A., Hara, T., McFadden, J. P., Halekas, J. S., Mitchell, D. L., … Jakosky, B. M. (2018). Cold dense ion outflow observed in the Martian-induced magnetotail by MAVEN. *Geophys. Res. Lett.*, *45*(11), 5283–5289. https://doi.org/10.1029/2018GL077584

Inui, S., Seki, K., Sakai, S., Brain, D. A., Hara, T., McFadden, J. P., Halekas, J. S., Mitchell D. L., DiBraccio G. A., and Jakosky B. M. (2019). Statistical study of heavy ion outflows from Mars observed in the Martian-induced magnetotail by MAVEN. *J. Geophys. Res.: Space Phys.*, *124*(7), 5482–5497. https://doi.org/10.1029/2018JA026452

Jakosky, B. M., and Phillips, R. J. (2001). Mars' volatile and climate history. *Nature*, *412*(6843), 237–244. https://doi.org/10.1038/35084184

Jakosky, B. M., Grebowsky, J. M., Luhmann, J. G., Connerney, J., Eparvier, F., Ergun, R., Halekas, J., Larson, D., Mahaffy, P., … Yelle, R. (2015a). MAVEN observations of the response of Mars to an interplanetary coronal mass ejection. *Science*, *350*(6261), aad0210. https://doi.org/10.1126/science.aad0210

Jakosky, B. M., Lin, R. P., Grebowsky, J. M., Luhmann, J. G., Mitchell, D. F., Beutelschies, G., Priser, T., Acuna, M., Andersson, L., … Zurek, R. (2015b). The Mars Atmosphere and Volatile Evolution (MAVEN) mission. *Space Sci. Rev.*, *195*(1–4), 3–48. https://doi.org/10.1007/s11214-015-0139-x

Li, S. B., Lu, H. Y., Cui, J., Yu, Y. Q., Mazelle, C., Li, Y., and Cao, J. B. (2020). Effects of a dipole-like crustal field on solar wind interaction with Mars. *Earth Planet. Phys.*, *4*(1), 23–31. https://doi.org/10.26464/epp2020005

Lillis, R. J., Brain, D. A., Bougher, S. W., Leblanc, F., Luhmann, J. G., Jakosky, B. M., Modolo, R., Fox, J., Deighan, J., … Lin, R. P. (2015). Characterizing atmospheric escape from Mars today and through time, with MAVEN. *Space Sci. Rev.*, *195*(1–4), 357–422. https://doi.org/10.1007/s11214-015-0165-8

Lin, R. T., Huang, S. Y., Yuan, Z. G., Jiang, K., Xu, S. B., Wei, Y. Y., Xiong, Q. Y., Zhang, J., Zhang, Z. H., … McFadden, J. (2021). Characteristics of energetic oxygen ions escaping from Mars: MAVEN observations. *J. Geophys. Res.: Space Phys.*, *126*(8), e2021JA029507. https://doi.org/10.1029/2021JA029507

Liu, Y., Nagy, A. F., Gombosi, T. I., DeZeeuw, D. L., and Powell, K. G. (2001). The solar wind interaction with Mars: results of three-dimensional three-species MHD studies. *Adv. Space Res.*, *27*(11), 1837–1846. https://doi.org/10.1016/S0273-1177(01)00301-5

Luhmann, J. G., Tatrallyay, M., and Pepin, R. O. (1992). *Venus and Mars: Atmospheres, Ionospheres, and Solar Wind Interactions*. Washington DC: American Geophysical Union. https://doi.org/10.1029/GM066

Lundin, R., Barabash, S., Fedorov, A., Holmström, M., Nilsson, H., Sauvaud, J. A., and Yamauchi, M. (2008). Solar forcing and planetary ion escape from Mars. *Geophys. Res. Lett.*, *35*(9), L09203. https://doi.org/10.1029/2007GL032884

Lundin, R., Barabash, S., Holmström, M., Nilsson, H., Yamauchi, M., Dubinin, E. M., and Fraenz, M. (2009). Atmospheric origin of cold ion escape from Mars. *Geophys. Res. Lett.*, *36*(17), L17202. https://doi.org/10.1029/2009GL039341

Lundin, R., Barabash, S., Yamauchi, M., Nilsson, H., and Brain, D. (2011). On the relation between plasma escape and the Martian crustal magnetic field. *Geophys. Res. Lett.*, *38*(2), L02102. https://doi.org/10.1029/2010GL046019

Matsunaga, K., Seki, K., Brain, D. A., Hara, T., Masunaga, K., Mcfadden, J. P., Halekas, J. S., Mitchell, D. L., Mazelle, C., … Jakosky, B. M. (2017). Statistical study of relations between the induced magnetosphere, ion composition, and pressure balance boundaries around Mars based on MAVEN observations. *J. Geophys. Res.: Space Phys.*, *122*(9), 9723–9737. https://doi.org/10.1002/2017JA024217

McFadden, J. P., Kortmann, O., Curtis, D., Dalton, G., Johnson, G., Abiad, R., Sterling, R., Hatch, K., Berg, P., … Jakosky, B. (2015). MAVEN suprathermal and thermal ion composition (STATIC) instrument. *Space Sci. Rev.*, *195*(1–4), 199–256. https://doi.org/10.1007/s11214-015-0175-6

Mendillo, M., Withers, P., Hinson, D., Rishbeth, H., and Reinisch, B. (2006). Effects of solar flares on the ionosphere of Mars. *Science*, *311*, 1135–1138. https://doi.org/10.1126/science.1122099

Morgan, D. D., Gurnett, D. A., Kirchner, D. L., David Winningham, J., Frahm, R. A., Brain, D. A., Mitchell, D. L., Luhmann, J. G., Nielsen, E., … Plaut, J. J. (2010). Radar absorption due to a corotating interaction region encounter with Mars detected by MARSIS. *Icarus*, *206*(1), 95–103. https://doi.org/10.1016/j.icarus.2009.03.008

Nilsson, H., Stenberg, G., Futaana, Y., Holmström, M., Barabash, S., Lundin, R., Edberg, N. J. T., and Fedorov, A. (2012). Ion distributions in the vicinity of Mars: Signatures of heating and acceleration processes. *Earth, Planets Space*, *64*(2), 135–148. https://doi.org/10.5047/eps.2011.04.011

Nilsson, H., Edberg, N. J. T., Stenberg, G., Barabash, S., Holmström, M., Futaana, Y., Lundin, R., and Fedorov, A. (2011). Heavy ion escape from Mars, influence from solar wind conditions and crustal magnetic fields. *Icarus*, *215*(2), 475–484. https://doi.org/10.1016/j.icarus.2011.08.003

Ramstad, R., Barabash, S., Futaana, Y., Nilsson, H., and Holmström, M. (2016). Effects of the crustal magnetic fields on the Martian atmospheric ion escape rate. *Geophys. Res. Lett.*, *43*(20), 10574–10579. https://doi.org/10.1002/2016GL070135

Trotignon, J. G., Mazelle, C., Bertucci, C., and Acuña, M. H. (2006). Martian shock and magnetic pile-up boundary positions and shapes determined from the Phobos 2 and Mars Global Surveyor data sets. *Planet. Space Sci.*, *54*(4), 357–369. https://doi.org/10.1016/j.pss.2006.01.003

Wang, Z. H., Guo, J. P., Feng, X. S., Liu, C. X., Huang, H., Lin, H. B., Tan C. M., Yan, Y.

H., and Wan, W. X. (2018). The merging of two stream interaction regions within 1 au: the possible role of magnetic reconnection. *Astrophys. J. Lett.*, *869*(1), L6. https://doi.org/10.3847/2041-8213/aaf398

Weber, T., Brain, D., Xu, S. S., Mitchell, D., Espley, J., Mazelle, C., McFadden, J. P., and Jakosky, B. (2021). Martian crustal field influence on O^+ and O_2^+ escape as measured by MAVEN. *J. Geophys. Res.*: *Space Phys.*, *126*(8), e2021JA029234. https://doi.org/10.1029/2021JA029234

Xu, S. S., Liemohn, M. W., Dong, C. F., Mitchell, D. L., Bougher, S. W., and Ma, Y. J. (2016a). Pressure and ion composition boundaries at Mars. *J. Geophys. Res.*: *Space Phys.*, *121*(7), 6417–6429. https://doi.org/10.1002/2016JA022644

Xu, S. S., Mitchell, D., Liemohn, M., Dong, C. F., Bougher, S., Fillingim, M., Lillis, R., McFadden, J., Mazelle, C., … Jakosky, B. (2016b). Deep nightside photoelectron observations by MAVEN SWEA: implications for Martian northern hemispheric magnetic topology and nightside ionosphere source. *Geophys. Res. Lett.*, *43*(17), 8876–8884. https://doi.org/10.1002/2016GL070527